ResearchGate

See discussions, stats, and author profiles for this publication at: https://www.researchgate.net/publication/369080969

Modelling movement artefacts in handheld laser speckle contrast imaging

Conference Paper · March 2023

DOI: 10.1117/12.2650617

CITATION
1

READS
14

4 authors, including:

Ata Chizari
University of Twente
28 PUBLICATIONS **761** CITATIONS
SEE PROFILE

Tom Knop
University of Twente
12 PUBLICATIONS **41** CITATIONS
SEE PROFILE

Wiendelt Steenbergen
University of Twente
304 PUBLICATIONS **7,516** CITATIONS
SEE PROFILE

Some of the authors of this publication are also working on these related projects:

A handheld device for optical microcirculatory perfusion imaging View project

PhD-track 2005-2008 View project

All content following this page was uploaded by Ata Chizari on 10 March 2023.

The user has requested enhancement of the downloaded file.

PROCEEDINGS OF SPIE

SPIEDigitalLibrary.org/conference-proceedings-of-spie

Modelling movement artefacts in handheld laser speckle contrast imaging

Ata Chizari, Wilson Tsong, Tom Knop, Wiendelt Steenbergen

Ata Chizari, Wilson Tsong, Tom Knop, Wiendelt Steenbergen, "Modelling movement artefacts in handheld laser speckle contrast imaging," Proc. SPIE 12378, Dynamics and Fluctuations in Biomedical Photonics XX, 1237804 (7 March 2023); doi: 10.1117/12.2650617

SPIE.

Event: SPIE BiOS, 2023, San Francisco, California, United States

Downloaded From: https://www.spiedigitallibrary.org/conference-proceedings-of-spie on 10 Mar 2023 Terms of Use: https://www.spiedigitallibrary.org/terms-of-use

Modelling movement artefacts in handheld laser speckle contrast imaging

Ata Chizari, Wilson Tsong, Tom Knop, Wiendelt Steenbergen*
Biomedical Photonic Imaging group, Technical Medical Centre, Faculty of Science and Technology, University of Twente, PO Box 217, 7500 AE Enschede, The Netherlands.

*w.steenbergen@utwente.nl; phone + 31 53 489 3160; https://people.utwente.nl/w.steenbergen

ABSTRACT

Progress has been made in laser speckle contrast imaging (LSCI) of microcirculatory blood flow for biology and medicine. However, the underlying reason for occurrence of movement artefacts (MA) that compromises effective use of LSCI remains largely unexplored. Here, employing a dual-camera setup for both speckle imaging and movement tracking, we validate our analytical model that is based on optical Doppler effect for predication of speckle contrast drop as a function of applied translational speed. We perform both motorized and handheld experiments where planar and scrambled wave illumination schemes have been examined. Experimental data points fairly match the theoretical predictions. These findings indicate that the vision-based movement detection during handheld LSCI is a preferable option. Moreover, the proposed analytical model is promising for further exploration of MA in order to realize a reliable handheld LSCI.

Keywords: Laser speckle contrast imaging, movement artefacts, motion artifacts, enhanced correlation coefficient maximization, ECC, optical Doppler effect, analytical modeling, numerical analysis.

1. INTRODUCTION

Laser speckle contrast imaging (LSCI) is a non-interventional, fast and affordable technique to assess relative microcirculatory blood flow. In this imaging technique, an expanding coherent laser beam is illuminated on the test object. Due to undergoing different pathlengths in the tissue, a random interference pattern will be observed on a camera which is called speckle. If the scattering medium is static, the observed speckle pattern will be static, too, and its normalized standard deviation (i.e. speckle contrast) will approach unity. The camera captures speckle patterns with a certain exposure time and due to the blood flow, the observed time-integrated speckle pattern will be blurred such that the higher the blood flow, the lower the speckle contrast. Since the first introduction of LSCI in 1980s[1], it is still an active field of study and becomes advanced in different aspects. Recently, LSCI has been employed in a wide range of medical applications including ophthalmology[2], brain[3], robot-assisted surgery[4], psoriasis[5,6] and plastic surgery[7].

Due to its noncontact nature, the LSCI measurements are influenced by environmental conditions such as movements of the subject[8,9]; this challenge is called movement artefacts (MA). Mounting an adjacent opaque surface[10] in the field-of-view (FOV) of the camera for speckle imaging was the first attempt to detect MA in a mounted setting during exercise[11]. An improved version of such opaque surface called bilayer adhesive was used to subtract the signal recorded on it from the measured perfusion[12]. A regression method was used to remove movement-related signal based on identification of an static object in a speckle image. The need for a compact and handheld device in clinical settings set off study of MA in handheld LSCI[13] where a so called fiducial marker was placed in the FOV[14]. A wireless LSCI system has been made for use in the operation room during free flap breast reconstruction[15]. Influence of scattering level of the medium as well as quantification of the hand-arm movement was studied[16]. Hardware-based image stabilization[17] and software-based image segmentation and stabilization[18] were introduced to enhance perfusion images obtained in handheld LSCI. Use of plane waves or spherical waves compared to the mostly used scrambled waves made by glass diffusers was shown to increase robustness of handheld LSCI against MA[19]. A systematic study was carried out by applying controlled movements on the test objects aiming to quantify movement artefacts and compare the performance of multi-exposure speckle imaging (MESI) with the conventional single-exposure LSCI in the MA context[20]. Also, influence of setup parameters in creation of MA in modulated laser and synthetic exposure LSCI has been investigated[21]. By tracking movements during handheld measurements directly on speckle images, MA corrected perfusion images were made based on local extrapolation of perfusion versus speed as well as spatial alignment of temporally averaged perfusion maps[22]. More recently, MA in a

Dynamics and Fluctuations in Biomedical Photonics XX, edited by Valery V. Tuchin, Martin J. Leahy, Ruikang K. Wang, Zeev Zalevsky, Proc. of SPIE Vol. 12378, 1237804 · © 2023 SPIE · 1605-7422 · doi: 10.1117/12.2650617

Downloaded From: https://www.spiedigitallibrary.org/conference-proceedings-of-spie on 10 Mar 2023
Terms of Use: https://www.spiedigitallibrary.org/terms-of-use

mounted setting has been investigated by dual-wavelength laser illumination, green (532 nm) for feature tracking by an RGB camera and red (680 nm) for speckle imaging by a monochromatic camera. By applying optical flow for motion tracking, spatial alignment of perfusion images has been carried out. Then, by giving low weighting factor to suddenly changing contrast values, the MA related perfusion images have been removed in liver mode.

In a previous study, we proposed a numerical model to fundamentally study the influence of wavefront types on MA caused by translation of a handheld LSCI[23]. In this study, we validate the proposed model using a dual-illumination dual-camera setup for measurement of the applied speed during movements both in motorized and handheld modes.

2. THEORY

Consider a solid object moving parallel to a pair of illumination and detection system with the speed $\vec{v}$. The temporal fluctuations of detected intensity at each spot on the detector is dictated by the optical Doppler shift defined as $\omega_D = \vec{v}.\left(\overrightarrow{k_s} - \overrightarrow{k_i}\right)$ where $\overrightarrow{k_i}$ is the cone of illumination wavevectors, that is, a single vector in case of plane waves, location dependent single vectors in case of spherical waves and location dependent cones of wavevectors in case of scrambled waves (see Fig. 2 of Chizari et al.[23]). The cone of $\overrightarrow{k_s}$ forms between a spot on the scattering surface and the aperture of the imaging system. The semicircular density functions for the incoming and outgoing wavevector density functions are defined as[23]

$$p_{-i,s}\left(\frac{\omega_D \lambda}{2\pi V}\right) = \frac{\lambda}{\pi^2 V \chi_{i,s}} \sqrt{1 - \left(\frac{\omega_D \lambda}{2\pi V \chi_{i,s}}\right)^2}, \tag{1}$$

where λ, V and χ are wavelength, absolute speed, and shape parameters, respectively. The speckle intensity correlation can be calculated from the wavevector density functions shown in (*1*) as

$$g^{(2)}(\tau) = 16 b_i^2 b_s^2 \left(\frac{J_1\left(\frac{\tau}{b_i}\right) J_1\left(\frac{\tau}{b_s}\right)}{\tau^2}\right)^2 + 1, \tag{2}$$

where $b_{i,s} = \lambda/(2\pi\, V \chi_{i,s})$ and J_1 is the Bessel function of the first kind[24] order 1. The contrast of time-integrated intensity is calculated from the intensity correlation shown in (2) as

$$C^2 = \frac{32 b_i b_s}{T} \int_0^T \frac{1}{\tau^4} J_1\left(\frac{\tau}{bi}\right)^2 J_1\left(\frac{\tau}{b_s}\right)^2 \left[1 - \frac{\tau}{T}\right] d\tau, \tag{3}$$

where T is the exposure time of the optical detector.

In experiments, after measuring the on-surface displacements $\Delta x(t)$ and $\Delta y(t)$ between subsequent RGB frames with acquisition times of $\Delta t'(t)$, the time-dependent absolute speed is calculated as

$$V(t) = \frac{\sqrt{\Delta x^2(t) + \Delta y^2(t)}}{\Delta t'(t)}. \tag{4}$$

3. MATERIALS AND METHODS

The employed experimental setup consists of an LSCI system (see Figure 1(a)) and a scattering surface mounted on a motorized stage.

3.1 Illumination systems

For speckle imaging, a 50mW continuous wave polarized laser ($\lambda = 660$ nm) with a coherence length of 95 m was used. Planar waves were created by mounting a pair of plano-concave lenses (Qioptiq, N-BK7, F=-6) and a 5 × beam expander (Thorlabs, GBEE05-B) in front of the laser beam. The scrambled waves were created by mounting a single plano-concave lens (Qioptiq, N-BK7, F=-6) followed by a 20° top-hat square engineered diffuser (Thorlabs ED1-S20-MD) and a 0.5 neutral density filter (Thorlabs, ND05A). For white light illumination, a 1 W power LED white connected to 3.3 Volts was

Downloaded From: https://www.spiedigitallibrary.org/conference-proceedings-of-spie on 10 Mar 2023
Terms of Use: https://www.spiedigitallibrary.org/terms-of-use

mounted on the LSCI probe. The measured optical powers at the sample's surface located 31 cm away from the front side of the LSCI probe for planar and scrambled waves were 39 μW and 58 μW , respectively.

3.2 Imaging systems

During each measurement, a pair of RGB (Basler ace, acA1920-150uc working at a rate of 160 Hz and 2.5 ms exposure time and a frame size of 256×256 px) and monochromatic (Basler ace, acA2040-55um working at a rate of 40 Hz and $T = 10$ ms exposure time and a frame size of 200×200 px) cameras operated simultaneously with a train of triggering pulses with pulse period $\Delta t' \approx 6$ ms sent by a microcontroller board (Arduino Micro). For RGB imaging, a camera objective (Schneider Apo-Xenoplan 1.4 Lens) with a focal length of 23 mm and a bandstop filter (Semrock, stopline notch 658) was used. This way, detection of laser light on the sample was effectively avoided. For speckle imaging, an objective lens (Fujinon HF16XA-5M) of 16 mm focal length followed by a bandpass filter (Thorlabs, FB660 10nm) and a linear polarizer (Thorlabs, LPNIRE 100B) directed perpendicular to the laser polarization were used. This way, the background light as well as the specular reflection of the laser light from the scattering surface on the mono camera was minimized. At the sample's surface, both cameras were of the same pixel ratio of 83 μm/px. Therefore, the detected on-surface speeds using RGB camera have been directly considered for the corresponding speckle images acquired by the monochromatic camera.

3.3 Scattering surface and motorized stage

A matte surface was prepared by spraying (Ecopaint Vintage, chalk paint spray 400 ml) on a surface 6 times with an interval of 20 minutes [16]. Parallel to the matte surface, a random QR code (1.29 mm dimension of each square side) was placed in order to create an ideal texture for the MATLAB R2022b toolbox[25] Enhanced correlation coefficient maximization (ECC) algorithm[26] (the number of levels for multi-resolution execution is 2, the type of geometric transformation is 'translation', the number of iterations is N = 20, and the initial transformation per frame is set to zero) to accurately follow the applied on-surface movements to be converted to the laser beam displacements on the scattering surface (i.e. $\Delta x(t)$ and $\Delta y(t)$). The sample was mounted on a translational stage (Zaber, X-LHM200A-E03) to apply a constant acceleration of 3 $\mathrm{mm/s^2}$ where the speed raised up to $V = 25$ mm/s during 8.5 seconds.

4. RESULTS

The probability density functions of the illumination and detection wavevectors introduced in (1) were created based on shape parameters related to the experimental setup. To model planar waves, there is a single wavevector; therefore, $\chi_i \to 0$ and the density function approaches a Dirac delta function (see Figure 1(b)). To model scrambled waves formed by a glass diffuser, we note that the one-sided Doppler shift created by the illumination wavevectors on each spot on the scattering surface assuming paraxial approximation is $\Delta\omega_{D_i} = 2\pi a_i V/(\lambda z_i)$, with $a_i = 2.8$ mm and $z_i = 34$ cm being the half-width-at-half-maximum of laser beam illuminated on the diffuser and the distance from diffuser surface to the scattering surface, respectively. We define $\chi_i = a_i/z_i$.

At the detection side, the one-sided Doppler shift created by the scattering wavevectors from each spot on the surface assuming paraxial approximation is $\Delta\omega_{D_s} = 2\pi a_s V/(\lambda z_s)$, with $a_s = f/f_\#$ being the pupil's radius defined as the fraction of objective's focal length (16 mm) to the set f-number[27] ($f_\# = 8$) and $z_s = 38$ cm being the distance from the scattering surface to the objective's pupil. We define $\chi_s = a_s/z_s$. Based on the created wavevector density functions for planar waves, a representative serie of intensity correlation functions (shown in (2)) has been depicted in Figure 1(c) for a range of absolute speeds. We can see that for a low applied speed ($V = 0.1$ mm/s), the intensity correlation function is almost independent of the time-lag and the larger the applied speed, the steeper the correlation function.

In Figure 1(d), contrast of time-integrated intensity ($T = 10$ ms) versus applied speed is shown. The solid curves are analytical functions resulted from (3) and the data points are obtained by motorized experiments for both planar and scrambled waves where C is the spatial contrast (normalized standard deviation) of the obtained speckle frames and V is the absolute speed calculated from (4). Here, p_s is the same for both illumination schemes; however, since p_{-i} for scrambled waves is wider than p_{-i} for planar waves (see Figure 1(b)), drop of C for a certain speed is higher in scrambled case than the drop of C in planar case[19]. Furthermore, the experimental data points fairly match the corresponding analytical curves, validating the derived model.

Downloaded From: https://www.spiedigitallibrary.org/conference-proceedings-of-spie on 10 Mar 2023
Terms of Use: https://www.spiedigitallibrary.org/terms-of-use

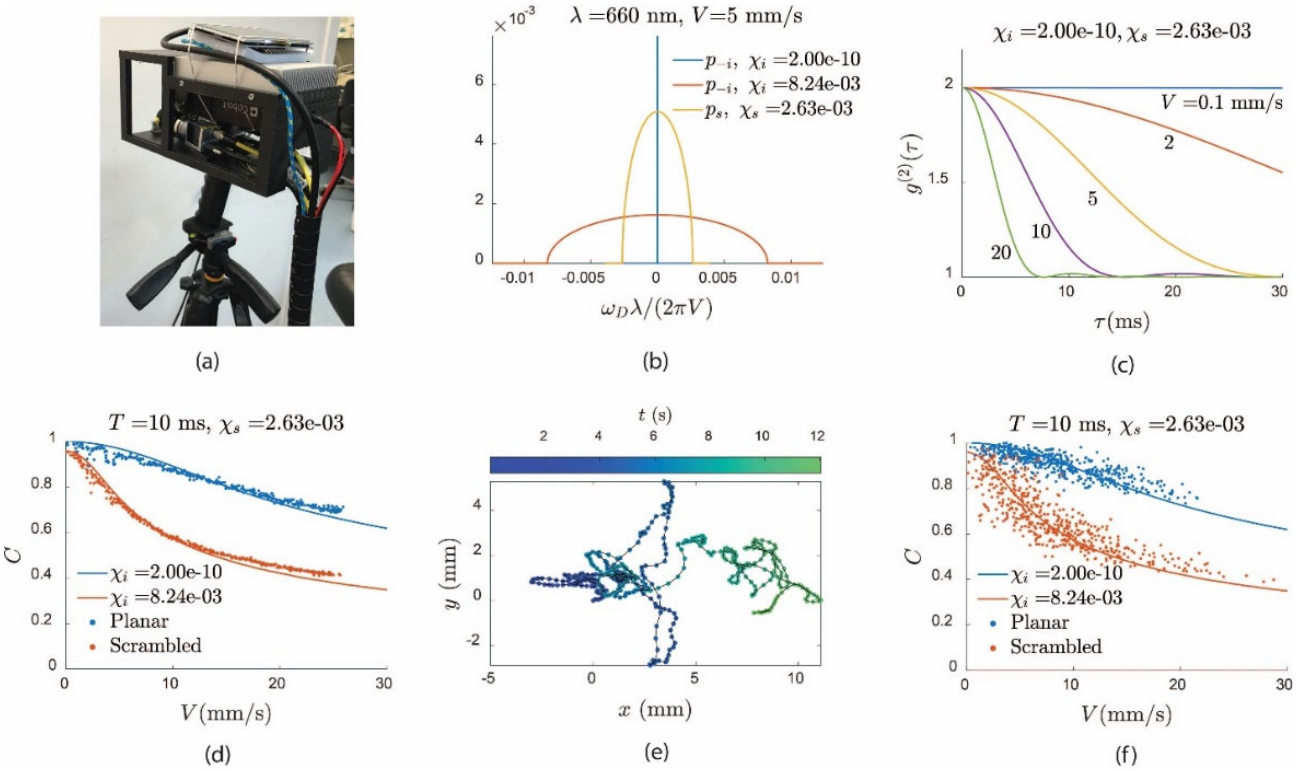

Figure 1 (a) LSCI device mounted on a tripod. (b) Wavevector density functions obtained from (1) to model planar waves (blue), scrambled waves (red), and imaging system (yellow). Intensity correlation as a function of time-lag obtained from (2) for a range of translational speeds. (d) Contrast of the time integrated intensity as a function of applied speed obtained from (3) modeling planar and scrambled waves. The data points in (d) represent experimental values in a motorized case in which translational speeds are calculated using (4). (e) Lissajous plot of detected $x-y$ (on-surface) displacements during a handheld measurement. (f) Speckle contrast as a function of detected speed in a handheld case. The solid curves in (f) are the same as (d).

Since it is ultimately a handheld experiment that matters, we performed handheld measurements of each 12 seconds duration. The calculated on-surface locations $x(t') = \int_0^{t'} \Delta x(t)dt$ and $y(t') = \int_0^{t'} \Delta y(t)dt$ have been shown in Figure 1(e) for the scrambled wave experiment which is a random pattern in mm scale. Similar to Figure 1(d), the speckle contrast versus applied speed has been shown in Figure 1(f) with the difference that the data points correspond to the handheld experiments. As opposed to the mounted case, the experimental data points are of higher deviations such that they form a cloud around the analytical curves. This is partly due to the error of the ECC algorithm and partly due to the error in synchronizing frames of the camera pair.

5. CONCLUSION

We presented a validation study for theoretical prediction of translation-based movement artefacts (MA) in laser speckle contrast imaging (LSCI) based on an optical Doppler shift model. Translational movements of a matte surface of high scattering coefficient was considered. Wavevector density functions for illumination and detection were first created. The shape parameters were chosen according to the experimental parameters. Then, the intensity correlation functions were calculated to show their relation with the applied translational speed. Contrast of time-integrated intensity versus the applied speed was analytically calculated for the two cases of planar and scrambled waves. Finally, a dual-camera setup was used to simultaneously perform speckle imaging and measuring the on-surface speed associated with each speckle image. ECC algorithm was used to measure on-surface displacements.

In an MA study, the ultimate goal is to predict speckle contrast drop as a result of applied movements in order to correct perfusion images. In this study, we have demonstrated the possibility of simultaneous speckle imaging and on-surface movement tracking. Moreover, we validated the proposed model for prediction of speckle contrast drop versus the

Downloaded From: https://www.spiedigitallibrary.org/conference-proceedings-of-spie on 10 Mar 2023
Terms of Use: https://www.spiedigitallibrary.org/terms-of-use

measured on-surface speed. This study paves the way for further research on MA by considering tissue level scattering samples specially those including internal movements and blood flow.

6. ACKNOWLEDGEMENT

This study was supported by the Open Technology program of the Netherlands Organization for Scientific Research (NWO), Domain Applied and Engineering Sciences, under grant number 14538.

REFERENCES

1. Fercher, A. F. & Briers, J. D. Flow visualization by means of single-exposure speckle photography. *Opt. Commun.* **37**, 326–330 (1981).
2. Bunke, J. *et al.* Hyperspectral and Laser Speckle Contrast Imaging for Monitoring the Effect of Epinephrine in Local Anesthetics in Oculoplastic Surgery. *Ophthal. Plast. Reconstr. Surg.* **38**, 462–468 (2022).
3. Cumsille, P., Lara, E., Verdugo-Hernández, P., Acurio, J. & Escudero, C. A robust quantitative approach for laser speckle contrast imaging perfusion analysis revealed anomalies in the brain blood flow in offspring mice of preeclampsia. *Microvasc. Res.* **144**, (2022).
4. Liu, Y. Z. *et al.* Utility and usability of laser speckle contrast imaging (LSCI) for displaying real-time tissue perfusion/blood flow in robot-assisted surgery (RAS): comparison to indocyanine green (ICG) and use in laparoscopic surgery. *Surg. Endosc.* (2022) doi:10.1007/s00464-022-09590-3.
5. Margouta, A. *et al.* Blunted Microvascular Reactivity in Psoriasis Patients in the Absence of Cardiovascular Disease, as Assessed by Laser Speckle Contrast Imaging. *Life* **12**, 1796 (2022).
6. Schaap, M. J. *et al.* Perfusion measured by laser speckle contrast imaging as a predictor for expansion of psoriasis lesions. *Ski. Res. Technol.* **28**, 104–110 (2022).
7. To, C. *et al.* Intraoperative Tissue Perfusion Measurement by Laser Speckle Imaging: A Potential Aid for Reducing Postoperative Complications in Free Flap Breast Reconstruction. *Plast. Reconstr. Surg.* **143**, 287e-292e (2019).
8. Mahé, G., Durand, S., Humeau-Heurtier, A., Leftheriotis, G. & Abraham, P. Impact of Experimental Conditions on Noncontact Laser Recordings in Microvascular Studies. *Microcirculation* **19**, 669–675 (2012).
9. Chizari, A. Handheld laser speckle contrast perfusion imaging. (University of Twente, 2021). doi:10.3990/1.9789036552394.
10. Mahé, G. *et al.* Laser speckle contrast imaging accurately measures blood flow over moving skin surfaces. *Microvasc. Res.* **81**, 183–188 (2011).
11. Mahe, G. *et al.* Cutaneous microvascular functional assessment during exercise: A novel approach using laser speckle contrast imaging. *Pflugers Arch. Eur. J. Physiol.* **465**, 451–458 (2013).
12. Omarjee, L. *et al.* Optimisation of movement detection and artifact removal during laser speckle contrast imaging. *Microvasc. Res.* **97**, 75–80 (2015).
13. Farraro, R., Fathi, O. & Choi, B. Handheld, point-of-care laser speckle imaging. *J. Biomed. Opt.* **21**, 094001 (2016).
14. Lertsakdadet, B. *et al.* Correcting for motion artifact in handheld laser speckle images. *J. Biomed. Opt.* **23**, 36006 (2018).
15. Teunissen, S. E. M. Wireless Laser Speckle Contrast Imaging during DIEP flap breast reconstruction : an evaluation of the first prototype Master Thesis Technical Medicine. (2022).
16. Chizari, A., Knop, T., Sirmacek, B., van der Heijden, F. & Steenbergen, W. Exploration of movement artefacts in handheld laser speckle contrast perfusion imaging. *Biomed. Opt. Express* **11**, 2352 (2020).
17. Lertsakdadet, B., Dunn, C., Bahani, A., Crouzet, C. & Choi, B. Handheld motion stabilized laser speckle imaging. *Biomed. Opt. Express* **10**, 5149 (2019).
18. Chizari, A. *et al.* Handheld versus mounted laser speckle contrast perfusion imaging demonstrated in psoriasis lesions. *Sci. Rep.* **11**, 1–13 (2021).
19. Chizari, A., Knop, T., Tsong, W., Schwieters, S. & Steenbergen, W. Influence of wavefront types on movement artefacts in handheld laser speckle contrast perfusion imaging. *OSA Contin.* **4**, 1875 (2021).
20. Amphan, D. Quantification and Detection of Motion Artifacts in Laser Speckle Contrast Imaging. (2022).
21. Chammas, M., Yu, C.-Y., Lin, H.-H. & Pain, F. Unwanted movement bias evaluation for multiple exposure

Downloaded From: https://www.spiedigitallibrary.org/conference-proceedings-of-spie on 10 Mar 2023
Terms of Use: https://www.spiedigitallibrary.org/terms-of-use

speckle imaging of blood flow using the synthetic exposure approach. 23 (2022) doi:10.1117/12.2620674.
22. Chizari, A., Schaap, M. J., Knop, T., Seyger, M. M. B. & Steenbergen, W. Reliability of handheld laser speckle contrast perfusion imaging demonstrated in psoriasis lesions. 34 (2022) doi:10.1117/12.2608663.
23. Chizari, A., Tsong, W., Steenbergen, W. & others. Modeling movement artefacts in handheld laser speckle contrast perfusion imaging: influence of wavefront types. in *Dynamics and Fluctuations in Biomedical Photonics XIX* vol. 11959 25–31 (2022).
24. Bowman, F. *Introduction to Bessel functions*. (Dover, 1958).
25. Evangelidis, G. IAT: A Matlab toolbox for image alignment. (2013).
26. Evangelidis, G. D. & Psarakis, E. Z. Parametric Image Alignment Using Enhanced Correlation Coefficient Maximization. *IEEE Trans. Pattern Anal. Mach. Intell.* **30**, 1858–1865 (2008).
27. Kolner, B. H. Generalization of the concepts of focal length and f-number to space and time. *J. Opt. Soc. Am. A Opt. Image Sci. Vis.* **11**, 3229–3233 (1994).

Downloaded From: https://www.spiedigitallibrary.org/conference-proceedings-of-spie on 10 Mar 2023
Terms of Use: https://www.spiedigitallibrary.org/terms-of-use